ELSEVIER

Influence of thermal stratification on the surfacing and clustering of floaters in free surface turbulence

Salvatore Lovecchio, Francesco Zonta, Alfredo Soldati *

Dept. of Elec., Manag. and Mechanical Eng., University of Udine, Udine, Italy
Department of Fluid Mechanics, CISM, 33100 Udine, Italy

ARTICLE INFO

ABSTRACT

The dispersion of floaters, small organic particles lighter than water, on the free surface of an open turbulent channel flow subject to thermal stratification is studied by Direct Numerical Simulation (DNS) of turbulence and Lagrangian Particle Tracking (LPT). Constant heat flux is maintained at the free surface of the channel, the bottom wall is adiabatic and the turbulent flow is driven by a pressure gradient. This archetypal flow setup mimics an environmentally plausible situation which can be found in terrestrial water bodies. The free surface turbulence characteristic of such flows has a strong influence on the distribution of the floaters: the objective of this work is to study the effect of different regimes of stable stratification on the surface distribution of floaters. The distribution of the floaters can possibly influence the transfer of chemical species across the water/atmosphere interface. Our results show that the modification of turbulence due to the thermal stratification strongly influences the settling velocity of floaters in the bulk of the flow. At the surface, stratification effects are also observed on the clustering of the floaters: the filamentary patterns of floaters observed in unstratified turbulence are progressively lost as thermal stratification increases, and the distribution of the floaters remains roughly two-dimensional.

© 2014 Elsevier Ltd. All rights reserved.

1. Introduction

The dispersion of floaters on the free surface of water bodies is a crucial process in many environmental and geophysical flows [1,3,9,10,20]. Floaters, as algae, plankton and aggregates of organic matter are extremely important in the process of species transfer across water/atmosphere interfaces and have been the object of a number of recent works which question whether an homogeneous or clustered distribution of these organic floaters on the open surfaces may have an impact on the overall fluxes of chemical species between atmosphere and open water bodies. These studies underlined the existence of several physical mechanisms that induce a non-homogeneous and clustered distribution, which is found to ultimately depend on the structures and the scales of the turbulent flow. Recently, Durham et al. [2] showed that a simple vortical flow can trigger the rapid accumulation of the floaters via the combined effect of the buoyancy, inertia and motility of the floaters. In a similar study, Martins Afonso et al. [14] considered the dynamics of the particles in a field representing a free surface flow populated by synthetic vortices and were able to show the features of the clustering of the particles.

The problem of the dispersion of the floaters in unstratified free-surface turbulence was also examined by Lovecchio et al. [12] who observed a non uniform distribution at the surface, where the floaters cluster into string-like structures. In this case, clustering is controlled by the dynamics of the free-surface turbulence, characterized by upwellings (structures caused by the impingement of bursts emanating from the bottom wall) and downwellings (downdrafts occurring in regions where adjacent upwellings interact). Floaters reach the surface entrained by the upwellings, later gather in the downwelling regions from which, forbidden to sink, they cannot escape. Lovecchio et al. [12] found that the clusters of the floaters evolve in time producing filamentary structures which are extremely persistent, and evolve over several surface renewal cycles [7]. Building on these results, our object in this paper is to study how the stable stratification of the fluid influences the distribution of the floaters at the free surface.

Stable stratification (i.e., fluid density decreasing with height) is known to be an important feature in a number of environmentally significant flows [4,5,11]. Compared to unstratified flows, the dynamics of turbulent transport and internal energy conversion in stratified flows is more complex because of the strong coupling between velocity and temperature [25,26]. One of the most

* Corresponding author at: Dept. of Elec., Manag. and Mechanical Eng., University of Udine, Udine, Italy. Tel.: +39 0432 558020; fax: +39 0432 558027.

E-mail address: soldati@uniud.it (A. Soldati).

interesting features produced by the thermal stratification in turbulence is the formation of Internal Gravity Waves (IGW): the less-buoyant (cold) fluid lifted upward by turbulence may bounce back due to the buoyancy force causing an oscillation (IGW). A specific analysis on the effect of the fluid stable stratification in an open channel flow has been done by Taylor et al. [22]. Relevant to this study, the authors observed the generation of a stable thermocline near the free surface overlying a well-mixed turbulent region located near the bottom wall. It is reasonable to hypothesize that the modulation of turbulence by thermal stratification may result in a different dispersion/segregation of the floaters.

In this study, we use Direct Numerical Simulation (DNS) and Lagrangian Particle Tracking (LPT) to analyze the surfacing and clustering of the floaters in free-surface stably-stratified turbulence. In the present flow configuration, the stable stratification is realized by imposing a constant heat flux at the free surface and an adiabatic condition at the bottom wall.

This paper is organized as follows. The problem statement, the governing equations and the numerical methodology required for the simulations are presented in Section 2. Section 3 is devoted to the analysis and discussion of relevant statistics obtained from simulations where the trajectories of the floaters in stratified turbulence are computed from DNS+LPT. The discussion will be focused on the analysis of the velocity/temperature fluid flow field, on the quantification of the surfacing of the floaters and on the computation of the clustering of the floaters at the free surface. Finally, the conclusions are drawn in Section 4.

2. Methodology

The physical problem considered in this study is the dispersion of the floaters in a thermally-stratified open channel flow with an undeformable free surface (free-surface turbulence). The reference geometry consists of two horizontal (infinite) flat parallel walls; the x-, y- and z-axis of the coordinate system point in the streamwise, spanwise and wall-normal directions. Indicating with h the channel height, the size of the channel is $2\pi h \times \pi h \times h$ in x, y and z, respectively. A sketch of the computational domain, together with the boundary conditions for the fluid (water) is given in Fig. 1. For the fluid velocity, no-slip (resp. no-stress) boundary conditions are enforced at the bottom (resp. top) boundary. Note that the effect of imposing a flat non-deformable surface does not alter significantly the strength of IGW, since the elevation of surface waves is typically smaller (<0.1) compared to the thickness of IGW. For the fluid temperature, a constant heat flux (resp. adiabatic condition) is enforced at the top (resp. bottom) boundary [22]. Note that periodicity is applied in x and y for both velocity and temperature. Due to the free surface heating, there is a negative temperature difference between the bottom and the top layers of

Table 1
Floater surfacing and clustering in stratified free-surface turbulence: summary of the simulation parameters.

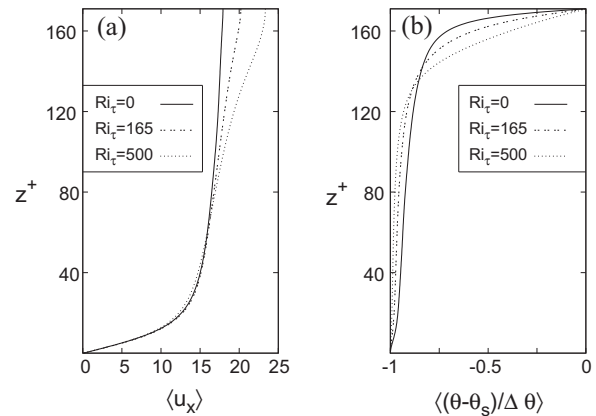| Simulation	Re_τ	Ri_τ	$S = \rho_p/\rho_f$	$St = \tau_p/\tau_f$
S1	171	0	0.5	0.063
			0.7	0.089
			0.8	0.102
			0.9	0.114
S2	171	165	0.5	0.063
			0.7	0.089
			0.8	0.102
			0.9	0.114
S3	171	500	0.5	0.063
			0.7	0.089
			0.8	0.102
			0.9	0.114

Fig. 2. Mean fluid streamwise velocity and temperature for stably-stratified free surface turbulence at $Ri_\tau = 0$ (solid line), $Ri_\tau = 165$ (dashed line) and $Ri_\tau = 500$ (dotted line). Panels: (a) mean fluid streamwise velocity, $\langle u_x \rangle$; (b) mean fluid temperature, $\langle (\theta - \theta_S)/\Delta\theta \rangle$.

the channel which causes a stable buoyancy effect (the gravitational acceleration g acting downward along the wall-normal direction). In dimensionless form the conservation of mass, momentum and energy of the fluid is described by the following set of three-dimensional time-dependent equations:

$$\nabla \cdot \mathbf{u} = 0, \tag{1}$$

$$\frac{\partial \mathbf{u}}{\partial t} + \mathbf{u} \cdot \nabla \mathbf{u} = \frac{1}{Re_\tau}\nabla^2 \mathbf{u} - \nabla p + \frac{Gr}{Re_\tau^2}\theta\delta_g + \delta_p, \tag{2}$$
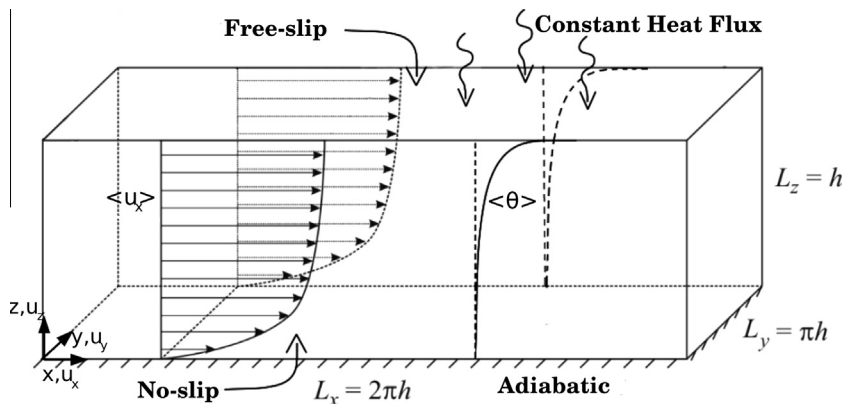

Fig. 1. Sketch of the computational domain with boundary conditions for the fluid velocity and temperature.

$$\frac{\partial \theta}{\partial t} + \mathbf{u} \cdot \nabla \theta = \frac{1}{Re_\tau Pr} \nabla^2 \theta - \beta_T, \tag{3}$$

where $\mathbf{u} = (u_x, u_y, u_z)$ is the velocity vector, p is the fluctuating kinematic pressure, $\delta_p = (1, 0, 0)$ is the mean pressure gradient that drives the flow in the streamwise direction, θ is the temperature field and $\delta_g = (0, 0, 1)$ is necessary to compute the buoyancy term only in the wall-normal direction. Eqs. (1)–(3) are subject to the following boundary conditions:

$$@ \text{ Wall}: u_x = u_y = u_z = 0, \quad \frac{\partial \theta}{\partial z} = 0 \tag{4}$$

$$@ \text{ Free} - \text{surface}: \frac{\partial u_x}{\partial z} = \frac{\partial u_y}{\partial z} = u_z = 0, \quad \frac{\partial \theta}{\partial z} = 1 \tag{5}$$

The dimensionless Reynolds, Grashof and Prandtl number are defined as

$$Re_\tau = \frac{u_\tau h}{\nu}, \quad Gr = \frac{g\beta h^3}{\nu^2} \frac{\partial \theta}{\partial z}\bigg|_s, \quad Pr = \frac{\mu c_p}{\lambda}. \tag{6}$$

where μ and ν are the dynamic and the kinematic viscosity, β is the thermal expansion coefficient, c_p is the specific heat and λ is the thermal conductivity. In the definition of Re_τ and Gr, $u_\tau = (h|\delta_p|/\rho)^{1/2}$ is the shear velocity (ρ being the fluid density) whereas $\partial \theta/\partial z|_s$ is the imposed free-surface heating. Note that $\beta_T = 1/(Re_\tau Pr)$ in Eq. (3), and depends on the specific flow configuration considered here (an open channel flow with a constant surface heating). Further details on this issue can be found in Appendix A. Eqs. (1)–(3) are discretized using a pseudo–spectral

Fig. 3. Root mean square (r.m.s.) of fluid velocity and temperature fluctuations for stably stratified free surface turbulence at different Ri_τ. Panels: (a) streamwise velocity fluctuations, $\langle u'_{x,rms} \rangle$; (b) spanwise velocity fluctuations, $\langle u'_{y,rms} \rangle$; (c) wall-normal velocity fluctuations, $\langle u'_{z,rms} \rangle$; (d) temperature fluctuations, $\langle \theta'_{rms} \rangle/\Delta\theta$.

method based on transforming the field variables into the wave-number space, through a Fourier representation for the periodic (homogeneous) directions x and y, and a Chebychev representation for the wall-normal (non-homogeneous) direction z. A two-level explicit Adams–Bashfort scheme for the non-linear terms and an implicit Crank–Nicolson method for the viscous terms are employed for the time advancement. As commonly done in pseudo-spectral methods, the convective non-linear terms are first computed in the physical space and then transformed in the wavenumber space using a de-aliasing procedure based on the 2/3-rule; derivatives are evaluated directly in the wavenumber space to maintain spectral accuracy. Further details can be found in [21,24,25].

The dynamics of the floaters is described by a set of ordinary differential equations for the position, x_p, and the velocity, v_p, of the floaters. In vector form:

$$\frac{d\mathbf{x}_p}{dt} = \mathbf{v}_p, \tag{7}$$

$$\frac{d\mathbf{v}_p}{dt} = \frac{(\rho_p - \rho)}{\rho_p}\mathbf{g} + \frac{(\mathbf{u}_{@p} - \mathbf{v}_p)}{\tau_p}(1 + 0.15 Re_p^{0.687}), \tag{8}$$

where $\mathbf{u}_{@p}$ is the fluid velocity at the position of the floater, interpolated with 6th-order Lagrange polynomials, whereas $\tau_p = \rho_p d_p^2/18\rho\nu$ is the relaxation time of the floater based on the density ρ_p and the diameter d_p of the floater. The Stokes drag coefficient is computed using a standard non-linear correction when the Reynolds number of the floater $Re_p = |\mathbf{u}_{@p} - \mathbf{v}_p|d_p/\nu > 0.2$. For thermally-stratified flows, the fluid density ρ in the equation of particle motion (Eq. (8)) depends on temperature. However, the variation of ρ with temperature is smaller compared with the difference between the density of the particle and the reference density of the fluid. This suggests that the variation of the fluid density in Eq. (8) is negligible, and ρ can be considered constant. Note also that, for the present choice of the physical parameters, the dynamics of the particles is not influenced by the lift force [6,16]. Floaters are treated as pointwise non-rotating rigid spheres (point–particle approach) and are injected into the flow at a concentration low enough to consider dilute system conditions: the effect of the floaters on turbulence is neglected (one-way coupling approach) as well as the inter-floaters collisions. Periodic boundary conditions are imposed on the floaters moving outside the computational domain in the homogeneous directions. In the wall-normal direction, the floaters reaching the free surface still obey the buoyancy force balance, whereas elastic rebound is enforced at the bottom wall. A 4th-order Runge–Kutta scheme is used to advance Eqs. (7) and (8) in time, starting from a two-dimensional random distribution of floaters (on the bottom plane, located at $z^+ = d_p^+/2$) with velocity $\mathbf{v}_p(t = 0) \equiv \mathbf{u}_{@p}(t = 0)$.

2.1. Summary of the simulations

An extensive campaign of Direct Numerical Simulations (DNS) is performed to investigate the role of the fluid stratification on the dispersion of the floaters with different inertia (see Table 1). All the simulations are run at reference Prandtl number $Pr = 5$ and Reynolds number $Re_\tau = 171$. Three different values of the Grashof number are considered in this study: $Gr = 0$, $Gr = 3.02 \times 10^5$ and $Gr = 9.15 \times 10^5$. As a consequence, the numerical simulations are run at three different values of the shear Richardson number $Ri_\tau = Gr/Re_\tau^2$, which measures the importance of buoyancy compared to inertia: $Ri_\tau = 0, Ri_\tau = 165$ and $Ri_\tau = 500$. Note that Gr is changed by changing the temperature gradient at the free surface. The spatial resolution of each simulation ($128 \times 128 \times 257$) is chosen to fulfill the requirements
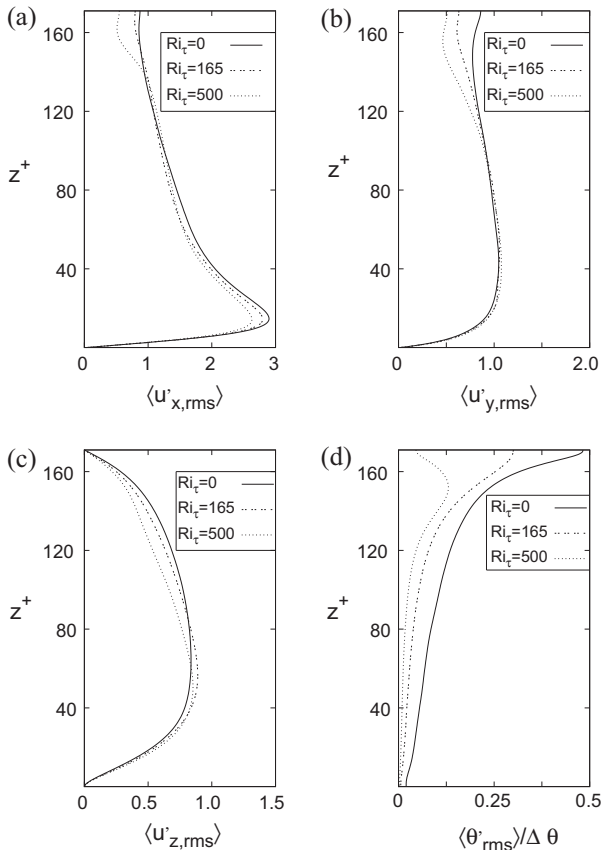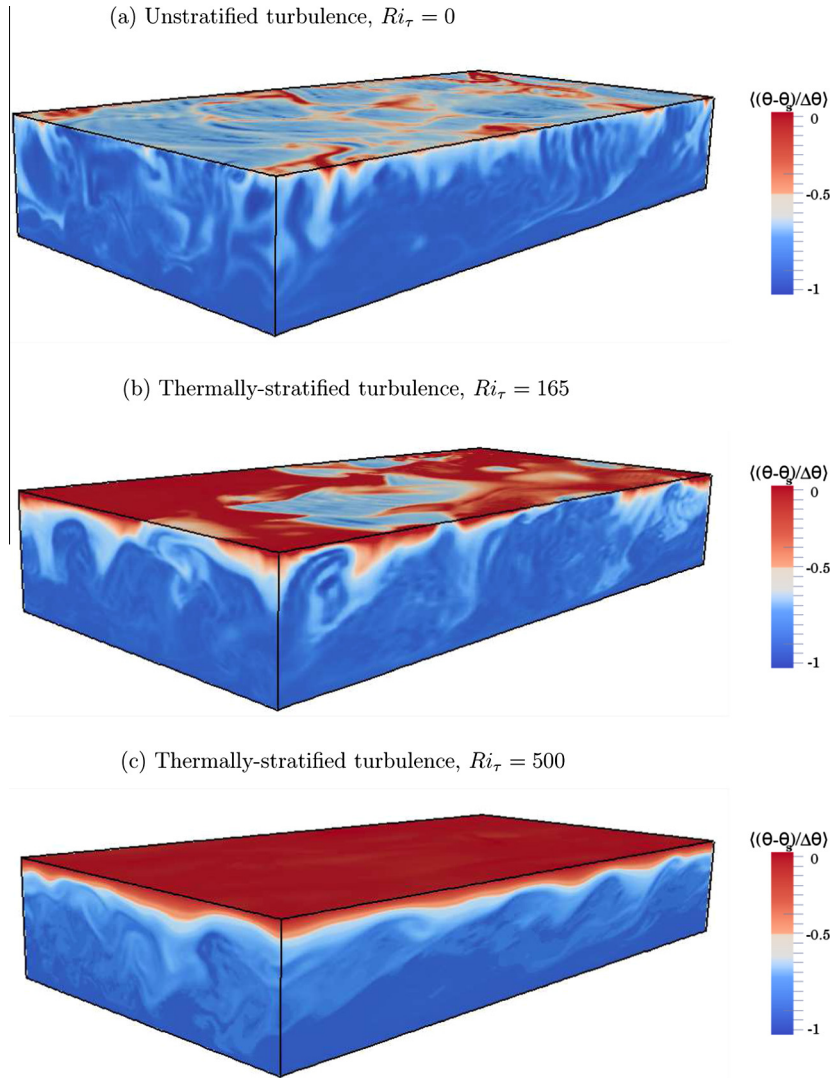
(a) Unstratified turbulence, $Ri_\tau = 0$

(b) Thermally-stratified turbulence, $Ri_\tau = 165$

(c) Thermally-stratified turbulence, $Ri_\tau = 500$

Fig. 4. Contour maps (three dimensional visualizations) of the temperature field. Panels: (a) simulation of unstratified turbulence ($Ri_\tau = 0$); (b) simulation of stratified turbulence ($Ri_\tau = 165$); (c) simulation of stratified turbulence ($Ri_\tau = 500$).

imposed by DNS [23]. To analyze the problem of the dispersion of the floaters, we consider samples of $N_P = 10^5$ floaters characterized by $d_p = 250\ \mu$m (a value in the size range of large phytoplankton cells, [18]) and by four different specific densities $S = \rho_p/\rho_f$: $S = 0.5, S = 0.7, S = 0.8$ and $S = 0.9$. The corresponding values of the non-dimensional response time of the floaters (Stokes number $St = \tau_p/\tau_f$, with $\tau_f = v/u_\tau^2$ the viscous timescale of the flow) ranges within $St = 0.06 \div 0.11$. A summary of the simulations parameters is provided in Table 1.

3. Results

3.1. Flow field and statistics

We consider first how the stable stratification of the fluid influences the mean flow field in free-surface turbulence. In Fig. 2(a) the mean streamwise velocity profile $\langle u_x \rangle$ (in wall units) is shown for the three regimes of stratification as a function of the wall-normal coordinate $z^+ = zu_\tau/v$. Brackets indicate time and space average. The averaging procedure is done using snapshots of velocity and temperature fields separated in time exceeding the correlation time and in space exceeding the integral scale. Since our

simulations are run keeping the driving pressure gradient constant, the slope of the velocity profile at the bottom wall is invariant among the different simulations. For increasing stratification, however, we observe a clear separation of the domain into two different regions: a turbulent region near the bottom wall ($z^+ < 80$), where the usual near wall-turbulence is maintained, and a buoyancy-affected region near the free surface ($z^+ > 80$), where the stratification becomes important and the flow velocity increases. The flow velocity and the corresponding mass flow rate increase near the free surface for increasing Ri_τ: this is due to a reduction of the wall-normal momentum transport, and in particular of the wall shear stress (the driving pressure gradient being constant in all the simulations). In Fig. 2(b) we show the behavior of the mean temperature profiles as a function of the wall-normal coordinate z^+. Regardless of the value of Ri_τ, we observe a region of large temperature gradient (near the free surface) topping a region where the temperature gradient is small and almost uniform ($z^+ < 80$). This region of well-mixed temperature near the bottom wall is due to the existence of active turbulence which effectively stirs the flow. The region near the free surface, characterized by the large temperature gradient and low mixing is usually called thermocline: the thickness of the thermocline increases with Ri_τ, possibly indicating that mixing is increasingly reduced. Fluid parcels
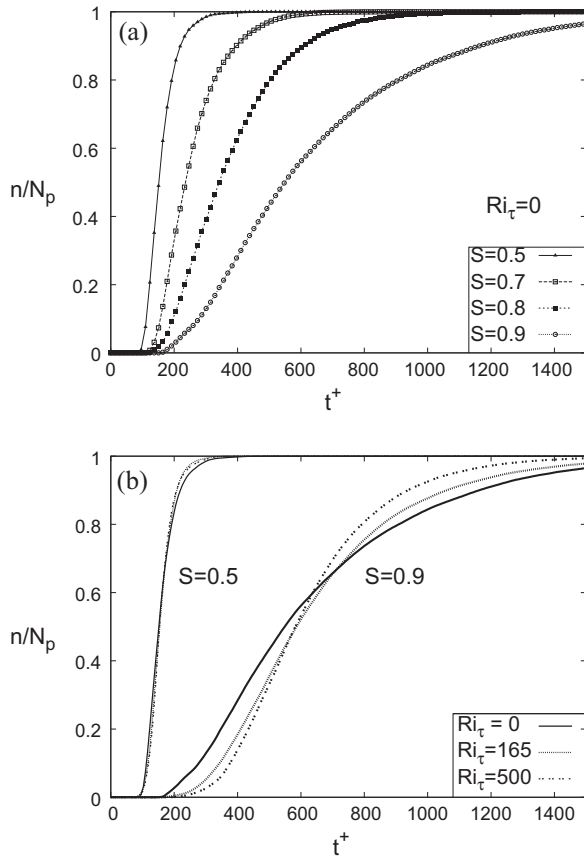
Fig. 5. Time behavior of the normalized number of floaters (n/N_P) settling at the free surface. Panels: (a) the effect of the floaters specific density (S) on n/N_P in unstratified turbulence ($Ri_\tau = 0$); (b) the effect of thermal stratification (Ri_τ) on n/N_P for $S = 0.5$ and $S = 0.9$.

Fig. 6. Probability density function (pdf) of floaters exit time (t_e^+). Panels: (a) the effect of floaters specific density (S) on $pdf(t_e^+)$ in unstratified turbulence ($Ri_\tau = 0$); (b) the effect of thermal stratification (Ri_τ) on $pdf(t_e^+)$ for $S = 0.9$.

approaching the thermocline from the lower turbulent region do not have enough momentum to trespass the gravitational potential barrier created by the steep temperature gradient of the thermocline.

To observe the influence of the stable stratification on mixing and turbulence characteristics, we examine the statistics of the fluid velocity and temperature fluctuations. The root mean square (rms) of the fluid velocity fluctuations in each direction is shown in Fig. 3(a)–(c). For unstratified turbulence ($Ri_\tau = 0$), the velocity fluctuations near the bottom wall (where turbulence production is maximum) are similar to those observed in standard closed channel simulations, indicating that the near wall turbulence is not influenced by the presence of a free-slip top boundary [8]. The largest effect of the free surface on turbulence is the increase of $\langle u'_{x,rms} \rangle$ and $\langle u'_{y,rms} \rangle$ near the surface itself. Correspondingly, $\langle u'_{z,rms} \rangle$ is largely reduced at the free surface and turbulence is nearly two-dimensional. For stratified turbulence ($Ri_\tau > 0$) we observe that the profiles of the velocity fluctuations are not altered in the near-wall region $z^+ < 40$, where the typical dynamics of the wall turbulence is maintained. A different situation occurs in the upper part of the domain ($z^+ > 90$), and in particular near the free surface. In this region, $\langle u'_{x,rms} \rangle$ and $\langle u'_{y,rms} \rangle$ decrease significantly as Ri_τ increases. This is due to the stabilizing effect induced by the fluid stratification, which reduces the turbulence fluctuations (turbulent kinetic energy is lost to potential energy). By contrast, $\langle u'_{z,rms} \rangle$ is less influenced by the fluid stratification near the free surface, owing to the strong constraint on u'_z imposed by the assumption of an undeformable free surface. This turbulence modulation has an impact on the distribution of temperature inside the
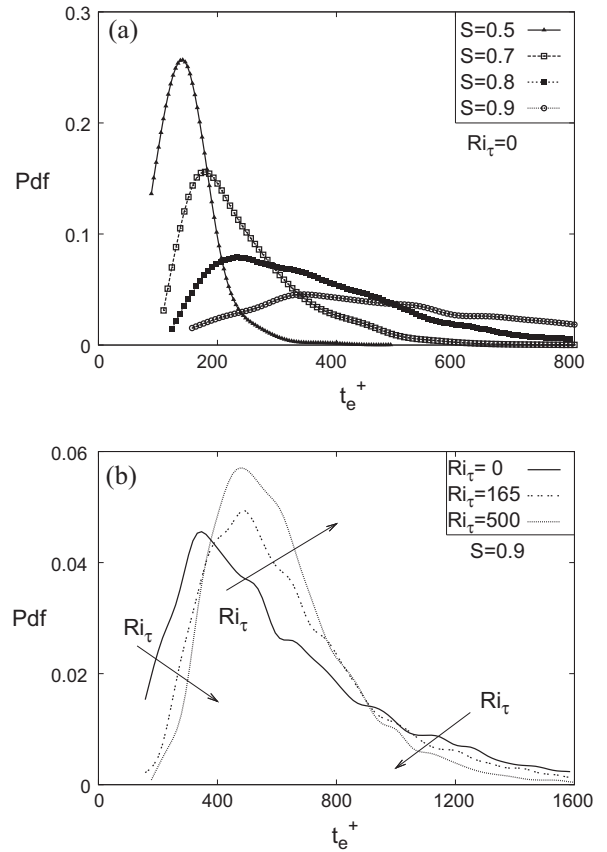
free-surface channel. The rms of the temperature fluctuations, $\theta'_{rms}/\Delta\theta$, is shown in Fig. 3(d). For neutrally buoyant and weakly-stratified flows ($Ri_\tau = 0$ and $Ri_\tau = 165$, respectively), the temperature fluctuations have a maximum at the free surface, or very close to it. This is due to the specific boundary condition prescribed for the energy equation (Eq. (3)): owing to the constant heat flux condition, there is no constraint on the temperature value at the interface, thus producing a maximum on the temperature fluctuations. This situation changes when the fluid stratification becomes stronger. For $Ri_\tau = 500$, we observe a peak value for the temperature fluctuations occurring at $z^+ \simeq 150$ (and not at the free surface). Higher temperature fluctuations below the free surface are not due to the turbulence structures; rather, they are the consequence of the large scale IGW occurring in this region when Ri_τ increases (see also the following discussion on flow structures). We also observe that $\theta'_{rms}/\Delta\theta$ decreases with increasing Ri_τ.

Flow visualizations are now considered to identify specific flow structures in free-surface stratified turbulence. In particular, we use contour maps of the temperature field, since the temperature distribution is a clear marker of the underlying flow field structure. Results, obtained for simulations run at $Ri_\tau = 0$, $Ri_\tau = 165$ and $Ri_\tau = 500$, are shown in Fig. 4. The mean flow is from left to right (positive x direction). For $Ri_\tau = 0$ (unstratified flow), temperature is passively advected by the velocity field. Bursts emanate from the bottom wall and produce upwelling motions of fluid traveling towards the free surface (blue regions in Fig. 4(a)). To replace the fluid carried by upwellings, downward motions (downwellings) are produced at the free surface and move towards the bulk region (red regions in Fig. 4(a)). These mechanisms for the velocity/temperature distribution change when considering a stratified flow.
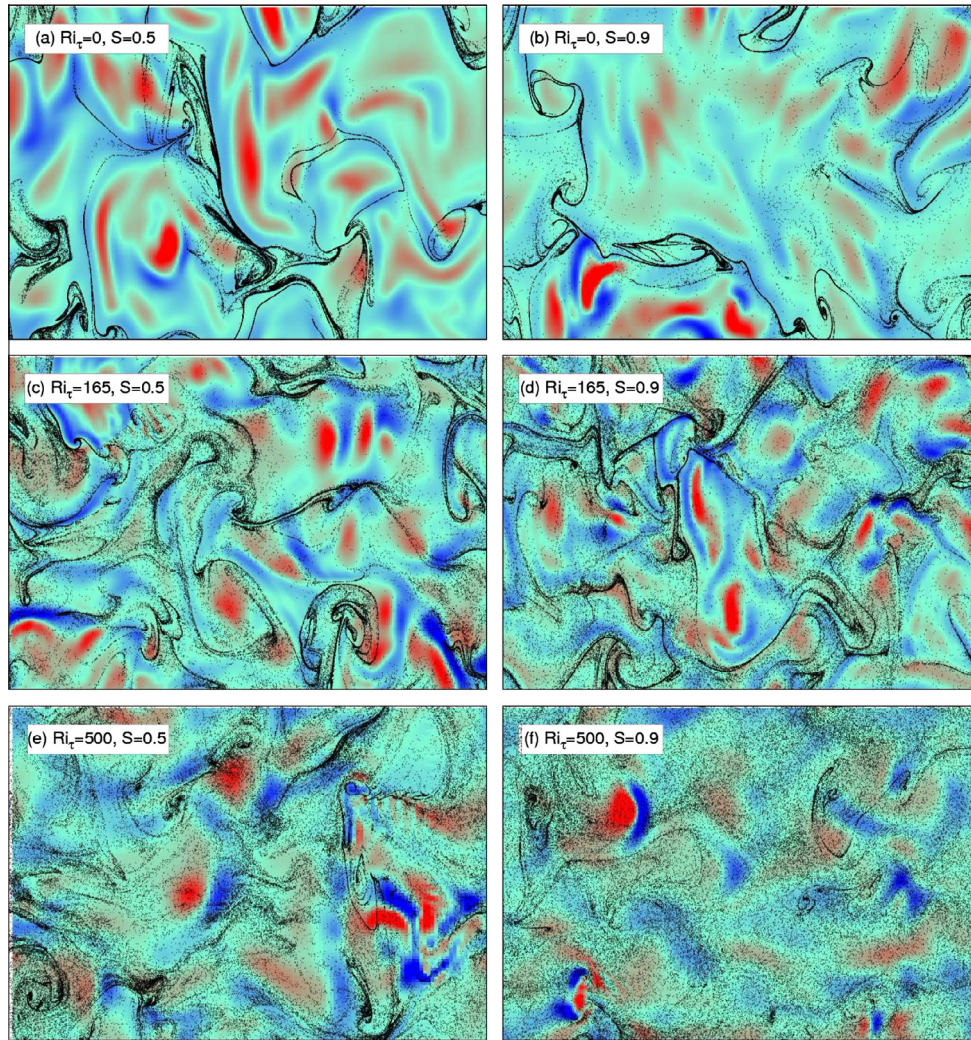
Fig. 7. Correlation between floater clusters and surface divergence ∇_{2D} for $Ri_\tau = 0, 165$ and 500 and for floater specific density $S = 0.5$ and $S = 0.9$. Panels: (a) $Ri_\tau = 0$ and $S = 0.5$; (b) $Ri_\tau = 0$ and $S = 0.9$; (c) $Ri_\tau = 165$ and $S = 0.5$; (d) $Ri_\tau = 165$ and $S = 0.9$; (e) $Ri_\tau = 500$ and $S = 0.5$; (f) $Ri_\tau = 500$ and $S = 0.9$.

Stratified flows can sustain a variety of wavy motions which have no counterpart in unstratified flows. The reason is the tendency for the vertical motions to be suppressed by buoyancy: a fluid particle which is displaced in the vertical direction by the velocity fluctuations tends to be restored to its original position; it may overshoot inertially and oscillate about this position [25]. This oscillation (IGW) is clearly visible near the free surface in Fig. 4(c). In the remaining part of the domain, intermittent bursts associated with the near-wall turbulence are seen. Note that the region where the internal waves are observed coincides with the region where a thermocline exists (see Fig. 2(b)), proving that the internal waves may be produced in a thermocline [4].

3.2. Floater surfacing

Floaters are initially positioned at the bottom wall and, being lighter than the fluid, rise towards the free surface. To quantify the surfacing process, we count the number of floaters n (normalized by the total number of floaters N_P) that have reached the free surface as a function of time t expressed in wall units ($t^+ = tu_\tau^2/\nu$). We computed n/N_P for each value of the specific density S. We start considering the case of floaters moving in unstratified turbulence ($Ri_\tau = 0$, Fig. 5(a)). Obviously, according to their specific density, those floaters with the lowest density are the first to reach the free surface. The surfacing process can be considered complete at

$t^+ \simeq 400$ for $S = 0.5$, at $t^+ \simeq 600$ for $S = 0.7$, at $t^+ \simeq 1000$ for $S = 0.8$ and at $t^+ > 1400$ for $S = 0.9$.

The effect of the thermal stratification on the surfacing of the floaters is shown in Fig. 5(b) just for the two cases in which the floaters have maximum and minimum rise velocity: $S = 0.5$ and $S = 0.9$. Since the effect of the fluid stratification on the surfacing of the floaters is more evident for the floaters with $S = 0.9$, we limit the discussion to this case. In the first part of the surfacing process, the fluid stratification prevents a larger number of floaters from reaching the free surface: at $t^+ \simeq 400$, $n/N_P \simeq 0.3$ for $Ri_\tau = 0$ and $n/N_P \simeq 0.15$ for $Ri_\tau = 500$ (a value half the size). In the second part of the surfacing process the situation reverses with the fluid stratification enhancing the number of the floaters that reach the free surface: at $t^+ > 1000$, $n/N_P \simeq 0.8$ for $Ri_\tau = 0$ and $n/N_P \simeq 0.9$ for $Ri_\tau = 500$. From a physical point of view, these results suggest that (i) the rise velocity of the faster floaters (those reaching the free surface before $t^+ = 400$) is reduced by the fluid stratification and that (ii) the rise velocity of the slower floaters is enhanced by the fluid stratification (those reaching the free surface after $t^+ = 1000$). This observation is necessarily related to the changes in the structure of turbulence, which is known to influence the rise velocity of light particles [13,15,18].

To characterize further the surfacing process, we quantify explicitly the time taken by each floater to reach the free surface, t_e. The probability distribution function (pdf) of t_e (expressed in
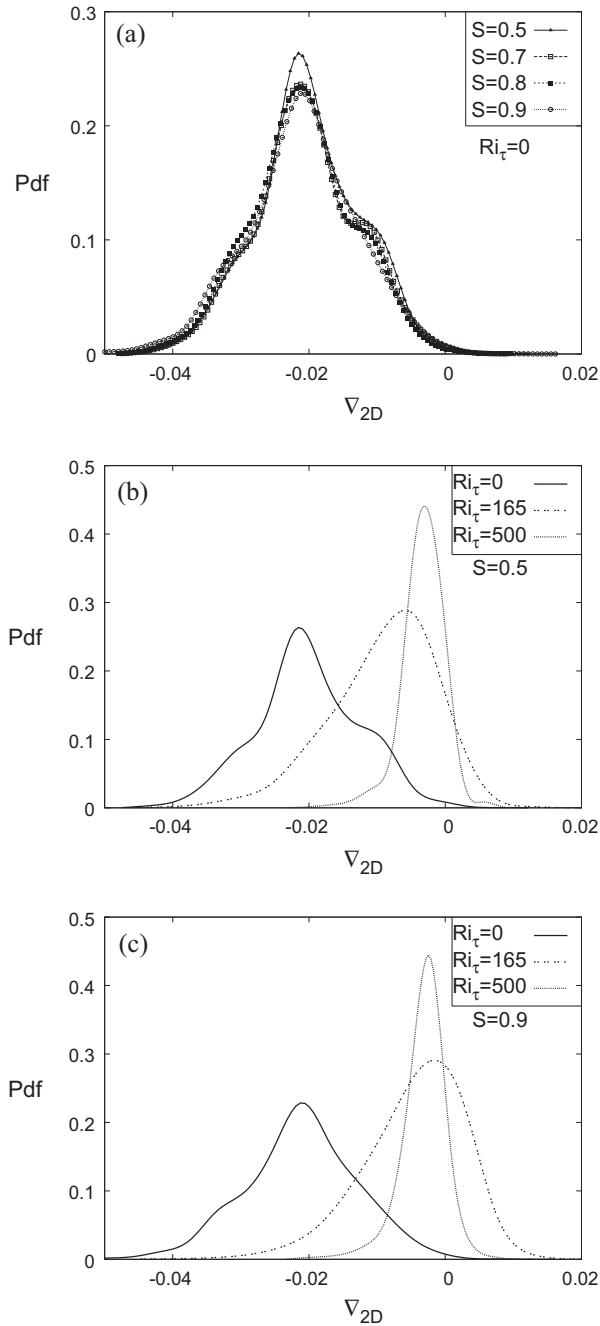
Fig. 8. Probability density function (pdf) of surface divergence ∇_{2D} computed at floaters position. Panels: (a) the effect of floaters specific density (S) on $pdf(\nabla_{2D})$ in unstratified turbulence; (b) the effect of thermal stratification (Ri_τ) on $pdf(\nabla_{2D})$ for $S = 0.5$; (c) the effect of thermal stratification (Ri_τ) on $pdf(\nabla_{2D})$ for $S = 0.9$.
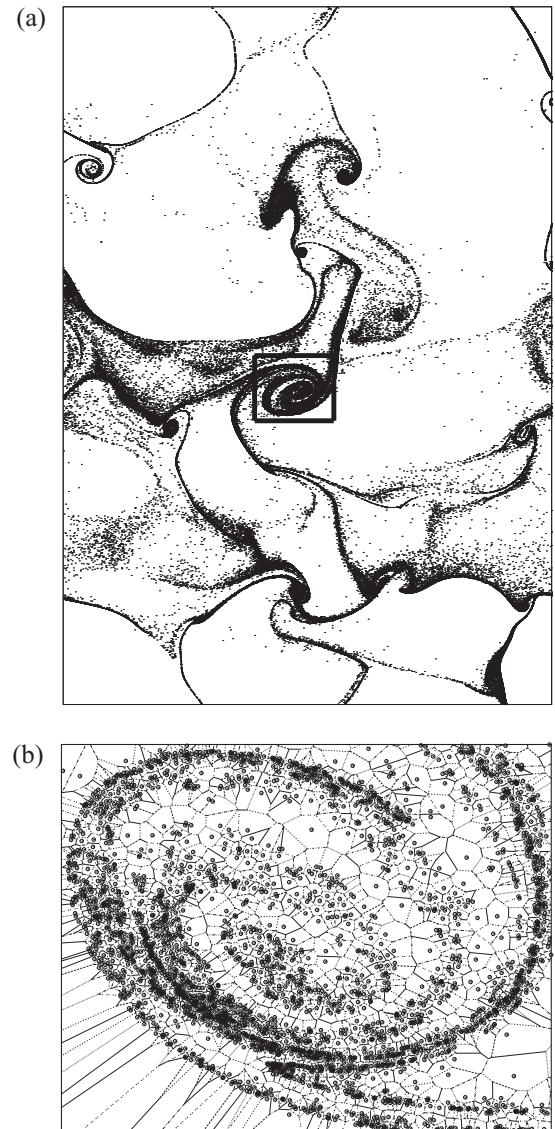

Fig. 9. Application of the Voronoi tessellation to the analysis of the clusters formed by the floaters. Panels: (a) Instantaneous distribution of the floaters at the free surface of the open channel for the case of $Ri_\tau = 0$ and $S = 0.5$; (b) Voronoi diagram corresponding to the small box indicated in Fig. 9(a).

wall units, t_e^+) is shown in Fig. 6. The abscissa of the maximum of the $pdf(t_e^+)$ is the expected value. For $Ri_\tau = 0$ (Fig. 6(a)), we observe that the expected value decreases for decreasing S (i.e., for increasing the buoyancy of the floater): the lower the density of the floater, the larger its buoyancy drift and the shorter the time taken to reach the surface (see also Fig. 5(a)). In particular, $t_e^+ \simeq 320, 220, 200$ and 150 for $S = 0.9, 0.8, 0.7$ and 0.5, respectively. We also note that, as the floater density becomes closer to that of the fluid ($S \to 1$), the $pdf(t_e^+)$ becomes broader, with decreasing $\max\{pdf(t_e^+)\}$ and higher tails: $\max\{pdf(t_e^+)\} \simeq 0.25, 0.15, 0.08$ and 0.05 for $S = 0.5, 0.7, 0.8$ and 0.9, respectively. The dynamics of the floaters with a stronger buoyancy is less

influenced by the turbulence fluctuations and the dispersion of the exit time (the tails of the $pdf(t_e^+)$) is reduced. Fig. 6(b) shows the distribution of the exit time of the floaters for $S = 0.9$ and different Richardson number Ri_τ (different fluid stratification): arrows point in the direction of increasing stratification (increasing Ri_τ). We observe that the expected value of t_e^+ increases for increasing stratification: from $t_e^+ = 350$ for $Ri_\tau = 0$ to $t_e^+ = 500$ for $Ri_\tau = 500$. Also, the value of $\max\{pdf(t_e^+)\}$ increases for increasing the fluid stratification, ranging from $\max\{pdf(t_e^+)\} \simeq 0.45$ for $Ri_\tau = 0$ to $\max\{pdf(t_e^+)\} \simeq 0.55$ for $Ri_\tau = 500$. These results indicate that the velocity of the faster floaters (those reaching the free surface at short times) in unstratified turbulence is larger compared to the corresponding value in stratified turbulence (but the number of floaters associated to this value of t_e^+ increases for increasing Ri_τ). Finally, we observe a crossover between the $pdf(t_e^+)$ curves occurring at $t_e^+ \simeq 900$: for unstratified turbulence, there is a significant number of floaters reaching the free surface at large time ($t_e^+ > 900$).
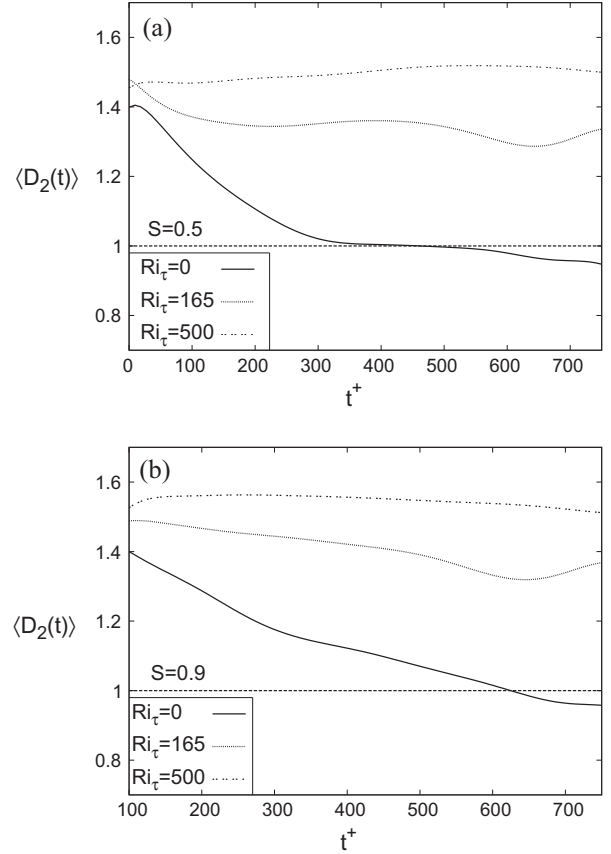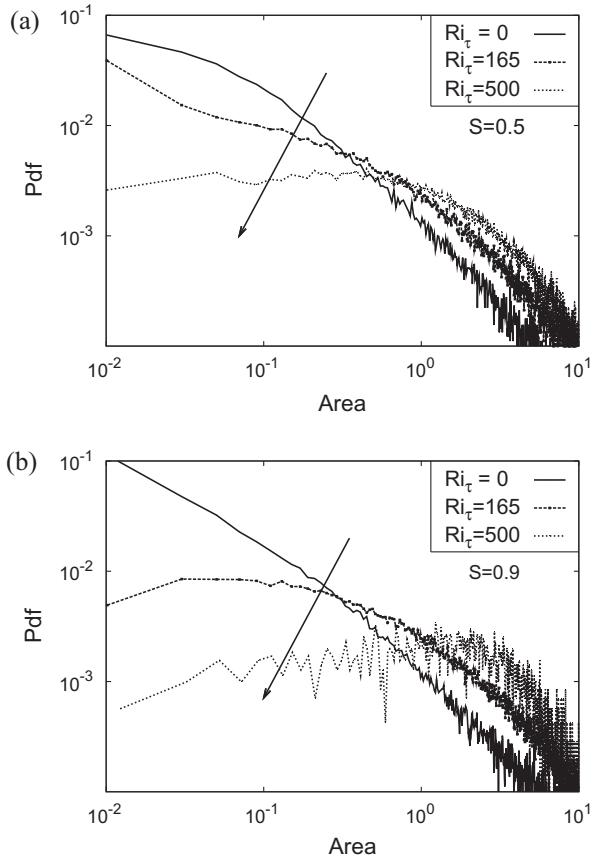
Fig. 10. Probability distribution function (pdf) of the Voronoi areas computed at the free surface for different Ri_τ. Panels: (a) $pdf(A)$ for floaters with specific density $S = 0.5$; (b) $pdf(A)$ for floaters with specific density $S = 0.9$.

Fig. 11. Time evolution of the cluster correlation dimension $\langle D_2(t) \rangle$ at the free surface for different Ri_τ. Panels: (a) $\langle D_2(t) \rangle$ for floaters with specific density $S = 0.5$; (b) $\langle D_2(t) \rangle$ for floaters with specific density $S = 0.9$.

3.3. Floater clustering

Once at the free surface, floaters cannot escape from it (due to their buoyancy) and their dynamics is closely related to the local structure of the velocity field. Turbulence at the free surface is nearly two dimensional, and can be characterized by the divergence of the velocity field [19,3]:

$$\nabla_{2D} = \frac{\partial u'}{\partial x} + \frac{\partial v'}{\partial y} = -\frac{\partial w'}{\partial z}. \tag{9}$$

In the present flow configuration $\nabla_{2D} \neq 0$ at the free surface. Therefore, floaters moving on the free surface probe a compressible system [1], where velocity sources are regions of local flow expansion ($\nabla_{2D} > 0$) generated by upwellings, and velocity sinks are regions of local flow compression ($\nabla_{2D} < 0$). In Fig. 7 we provide a qualitative characterization of the clustering of the floaters on the free surface by correlating the instantaneous position of the floaters with the contour maps of ∇_{2D}.

In particular, we consider the behavior of floaters with $S = 0.5$ (left panels) and $S = 0.9$ (right panels) for $Ri_\tau = 0$ (Fig. 7(a) and (b)), $Ri_\tau = 165$ (Fig. 7(d)) and $Ri_\tau = 500$ (Fig. 7(e) and (f)). To compare the results obtained with the same number of floaters settled at the free surface, the distribution of the floaters in Fig. 7 are computed at different t^+, depending on the specific density of the floaters: $t^+ \simeq 200$ for $S = 0.5$ and $t^+ \simeq 1000$ for $S = 0.9$ (this corresponds to $n/N_P \simeq 0.8$, see Fig. 5(b)). For $Ri_\tau = 0$ (Fig. 7(a) and (b)) we observe that the floaters escape velocity sources (red areas in Fig. 7(b)) and collect into velocity sinks (blue areas in Fig. 7(a) and (b)). Once trapped in these regions, the floaters

organize in clusters that are stretched by the fluid forming filamentary structures: these filaments of floaters correlate very well with the behavior of $\nabla_{2D} < 0$ [12]. The situation changes when considering a stratified fluid. Upwellings/downwellings at the free surface are less intense and the filamentary structures less evident, floaters being homogeneously distributed (Fig. 7(c)–(f)). To quantify these observations, we computed the probability of finding a floater in a flow region characterized by a specific value of $\nabla_{2D}, pdf(\nabla_{2D})$. For $Ri_\tau = 0$ (Fig. 8(a)), we clearly observe that floaters accumulate in regions of $\nabla_{2D} < 0$ (downwellings). This result does not depend on *the* floater buoyancy since, for all values of S, $\max\{pdf(\nabla_{2D})\} \simeq 0.25$ occurs for $\nabla_{2D} \simeq -0.02$. The effect of the fluid stratification on the clustering of the floaters at the surface is shown in Fig. 8(b) and (c), where we present the behavior of $pdf(\nabla_{2D})$ at varying Ri_τ and for the specific densities $S = 0.5$ (in Fig. 8(b)) and $S = 0.9$ (in Fig. 8(c)). As Ri_τ increases, we observe a clear displacement of the maximum of the pdf towards larger values of ∇_{2D} (Fig. 8(b) and (c)). This corresponds to a physical situation in which the accumulation of the floaters into downwellings (∇_{2D}) does not occur, and the floaters are distributed more homogeneously over the free surface. To quantify further the segregation of the floaters observed in Fig. 7, we use the Voronoi diagram [17]. The Voronoi diagram is a decomposition of the 2D surface into independent cells built around each floater. The area of each cell is therefore a measure of the local particle concentration: small areas indicate high concentration of the floaters, whereas large areas indicate low concentration of the floaters (see Fig. 9). In Fig. 10, we show the probability distribution function (pdf) of the Voronoi areas obtained by applying a Voronoi tessellation to the distribution of floaters shown in Fig. 7. In particular, Fig. 10(a)

refers to the situation observed in Fig. 7(a), (c), and (e) ($S = 0.5$), whereas Fig. 10(b) refers to the situation observed in Fig. 7(b), (d), and (f) ($S = 0.9$). Regardless of the value of S, we obtain similar trends for the probability distribution function of the Voronoi areas. For $Ri_\tau = 0$, we note that the maximum of the pdf curves occurs for very small areas. This reflects a situation in which floaters cluster in regions characterized by a very high concentration. For increasing stratification, the situation changes and the values of the Voronoi areas increase, thus meaning that the clustering of the floaters is damped (i.e., the area surrounding each floater is larger). This confirms the qualitative observation (Fig. 7) that the thermal stratification imposed throughout the channel reduces the clustering of the floaters at the surface. Finally, we characterize the topology of the clusters at the free surface by computing the time evolution of the correlation dimension of clusters, $D_2(t)$ (Fig. 11). The correlation dimension is a measure of the topological features of the distribution of the floaters. For simple geometrical structures like points, lines and surfaces, $D_2(t) = 0, 1, 2$, respectively. We compute the behavior of $D_2(t)$ for the floaters with $S = 0.5$ and $S = 0.9$ and for all the values of Ri_τ, starting the calculation when the floaters reach the free surface ($t^+ > 50$ for $S = 0.5$ and $t^+ > 150$ for $S = 0.9$, see Fig. 5(b)). We discuss our results considering $S = 0.5$ (Fig. 11(a)). For $Ri_\tau = 0, D_2(t)(@t = 0) \simeq 1.4$ and decays in time almost exponentially towards $D_2(t) \simeq 1$. The initial value of $D_2(t)(@t = 0)$ is lower than in [12] because here floaters are released from a plane close to the bottom wall and arrive at the free surface already segregated. Therefore, a segregation due to inertia is observed during the surfacing process. Once at the free surface, floaters segregate due to buoyancy. In a long-term limit $D_2(t) \simeq 1$, meaning that the floaters accumulate into filaments, i.e., line-like structures (see also Fig. 7a-b for a clear visualization of this result). For $Ri_\tau > 0, D_2(t)(@t = 0) \simeq 1.5$ and does not decay in time. This reflects the physical observation that the filaments of the floaters in thermally-stratified flows are hardly seen (see also Fig. 7(f)) and the distribution of the floaters remains roughly two dimensional ($D_2(t) \simeq 1.5$). The segregation of the floaters into filaments for unstratified turbulence is due to the combined dynamics of upwelling/downwelling events. For stratified turbulence, upwellings and downwellings lose momentum to trespass the potential barrier created near the free surface by the temperature gradient. Therefore, it is clear that the homogeneous distribution of the floaters for stratified turbulence stems from the weakening of upwellings and downwellings.

4. Conclusions

In this study, we used Direct Numerical Simulation and Lagrangian Particle Tracking to analyze the surfacing and the clustering of the floaters in a stably-stratified free-surface flow. In the present physical configuration, the flow is driven by a constant pressure gradient and the stable stratification is realized by imposing a constant heat flux at the free surface and an adiabatic condition at the bottom wall. Simulations were run at Prandtl number $Pr = 5$, shear Richardson number $Ri_\tau = 0, 165, 500$ and considering floaters with a specific density ratio $S = 0.5, 0.7, 0.8$ and 0.9. Flow statistics reveal that the imposed stable stratification suppresses the vertical transport of momentum and heat compared to the unstratified case, where temperature is a passive scalar. Using flow field visualizations we found that Internal Gravity Waves may be generated (for sufficiently high Ri_τ) near the free surface, whereas active turbulent bursting phenomena still occur near the bottom wall. Flow field modifications induced by the thermal stratification influence both the surfacing and clustering of the floaters at the surface. In particular, regardless of S, the fluid stratification focuses the range of the values that can be attained by the rise velocity of the floaters. This indicates that the vertical spread of the floater swarms induced by turbulence is decreased. Once at the surface, the fluid stratification prevents the formation of filamentary structures (observed in unstratified turbulence) and produces a nearly (two-dimensional) homogeneous distribution. This behavior is associated to a weakening of upwelling/downwelling events produced by the near-wall bursting phenomena.

Appendix A. Temperature flux balance

The temperature field inside the channel may be written as:

$$\theta = \theta_1(t) + \theta(\mathbf{x}, \mathbf{t}), \tag{10}$$

where θ_1 is the deterministic temperature field (which increases in time owing to the imposed surface heating), while $\theta(\mathbf{x}, \mathbf{t})$ is the turbulent temperature field (statistically steady). The substitution of Eq. (10) into the energy equation

$$\frac{\partial\theta}{\partial t} = -\mathbf{u} \cdot \nabla\theta + \frac{1}{Re_\tau Pr}\nabla^2\theta \tag{11}$$

gives

$$\frac{d\theta_1}{dt} + \frac{\partial\theta}{\partial t} = -\mathbf{u} \cdot \nabla\theta + \frac{1}{Re_\tau Pr}\nabla^2\theta. \tag{12}$$

Using the Reynolds average, Eq. (12) becomes

$$\frac{d\theta_1}{dt} = -\frac{\partial\langle\theta' u_z'\rangle}{\partial z} + \frac{1}{Re_\tau Pr}\frac{\partial^2\langle\theta\rangle}{\partial z^2}. \tag{13}$$

The right-hand side (rhs) of Eq. (13) is only a function of space (since $\theta(\mathbf{x}, \mathbf{t})$ is a statistically steady field) while the left-hand side (lhs) is only a function of time. As a consequence, Eq. (13) is satisfied only when rhs and lhs are constant. To compute the value of the constant, we integrate Eq. (13) from $z = 0$ (wall, subscript w) to $z = 1$ (free-surface, subscript s):

$$\int_0^1 \frac{d\theta_1}{dt}dz = \frac{1}{Re_\tau Pr}\left[\left.\frac{\partial\theta}{\partial z}\right|_s - \left.\frac{\partial\theta}{\partial z}\right|_w\right]. \tag{14}$$

Using the boundary conditions (see Eqs. (4) and (5)), we obtain

$$\frac{d\theta_1}{dt} = \frac{1}{Re_\tau Pr} \tag{15}$$

and

$$\theta_1(t) = \frac{t}{Re_\tau Pr} + C. \tag{16}$$

From Eq. (16) we note that the deterministic temperature field θ_1 increases linearly in time. Since we are interested in the behavior of the turbulent temperature field θ only, we subtract the temperature changes due to θ_1 from the energy balance equation. Therefore, the governing balance equation for the temperature field (Eq. (3)) becomes:

$$\frac{\partial\theta}{\partial t} + \mathbf{u} \cdot \nabla\theta = \frac{1}{Re_\tau Pr}\nabla^2\theta - \beta_T, \tag{17}$$

where $\beta_T = d\theta_1/dt = 1/Re_\tau Pr$.

References

[1] Cressman JR, Davoudi J, Goldburg WI, Schumacher J. Eulerian and Lagrangian studies in surface flow turbulence. New J Phys 2004;6:53. http://dx.doi.org/10.1088/1367-2630/6/1/053.

[2] Durham WM, Climent E, Stoker R. Gyrotaxis in a steady vortical flow. Phys Rev Lett 2011;106:238102. http://dx.doi.org/10.1103/PhysRevLett.106.238102.

[3] Eckhardt B, Schumacher J. Turbulence and passive scalar transport in a free-slip surface. Phys Rev E 2001;64:016314. http://dx.doi.org/10.1103/PhysRevE.64.016314.

[4] Ferziger JH, Koseff JR, Monismith SG. Numerical simulation of geophysical turbulence. Comput Fluids 2002;31:557. http://dx.doi.org/10.1016/S0045-7930(01)00066-4.

[5] Fritts DC, Alexander MJ. Gravity wave dynamics and effects in the middle atmosphere. Rev Geophys 2003;41:1003. http://dx.doi.org/10.1029/2001RG000106.

[6] Giusti A, Lucci F, Soldati A. Influence of the lift force in direct numerical simulation of upward/downward turbulent channel flow laden with surfactant contaminated microbubbles. Chem Eng Sci 2005;60:6176. http://dx.doi.org/10.1016/j.ces.2005.02.019.

[7] Komori S, Murakami Y, Ueda H. The relationship between surface-renewal and bursting motions in an open-channel flow. J Fluid Mech 1989;203:103. http://dx.doi.org/10.1017/S0022112089001394.

[8] Lam K, Banerjee S. On the condition of streak formation in bounded flows. Phys Fluids A 1992;4:306–20. http://dx.doi.org/10.1063/1.858306.

[9] Larkin J, Bandi MM, Pumir A, Goldburg WI. Power-law distributions of particle concentration in free-surface flows. Phys Rev E 2009;80:066301. http://dx.doi.org/10.1103/PhysRevE.80.066301.

[10] Larkin J, Goldburg WI, Bandi MM. Time-evolution of a fractal distribution: particle concentrations in free-surface turbulence. Physica D 2010;239:1264. http://dx.doi.org/10.1016/j.physd.2009.11.005.

[11] Lien R, Sanford TB. Turbulence spectra and local similarity scaling in a strongly stratified oceanic bottom boundary layer. Cont Shelf Res 2004;24:375. http://dx.doi.org/10.1016/j.csr.2003.10.007.

[12] Lovecchio S, Marchioli C, Soldati A. Time persistence of floating-particle clusters in free-surface turbulence. Phys Rev E 2013;88:033003. http://dx.doi.org/10.1103/PhysRevE.88.033003.

[13] Marchioli C, Fantoni M, Soldati A. Influence of added mass on anomalous high rise velocity of light particles in cellular flow field. A note on the paper of Maxey (1987). Phys Fluids 2007;19:098101. http://dx.doi.org/10.1063/1.2759528.

[14] Martins Afonso M, Mazzino A, Olla P. Renormalized transport of inertial particles in surface flows. J Phys A Math Theor 2009;42(27):275502. http://dx.doi.org/10.1088/1751-8113/42/27/275502.

[15] Maxey MR. The gravitational settling of aerosol particles in homogeneous turbulence and random flow fields. J Fluid Mech 1987;174:441. http://dx.doi.org/10.1017/S0022112087000193.

[16] Molin D, Marchioli C, Soldati A. Turbulence modulation and microbubble dynamics in vertical channel flow. Int J Multiphase Flow 2012;42:80. http://dx.doi.org/10.1016/j.ijmultiphaseflow.2012.01.010.

[17] Monchaux R, Bourgoin M, Cartellier A. Preferential concentration of heavy particles: a Voronoi analysis. Phys Fluids 2010;22:103304. http://dx.doi.org/10.1063/1.3489987.

[18] Ruiz J, Macias D, Peters F. Turbulence increases the average settling velocity of phytoplankton cells. Proc Natl Acad Sci USA 2004;101:17720. http://dx.doi.org/10.1073/pnas.0401539101.

[19] Schumacher J. Probing surface flows with Lagrangian tracers. Prog Theor Phys Suppl 2003;150:255. http://dx.doi.org/10.1143/PTPS.150.255.

[20] Singh P, Joseph DD, Aubry N. Dispersion and attraction of particles floating on fluid liquid surfaces. Soft Matter 2010;6:4310. http://dx.doi.org/10.1039/C000495M.

[21] Soldati A, Banerjee S. Turbulence modification by large-scale organized electrohydrodynamic flows. Phys Fluids 1998;10:1743. http://dx.doi.org/10.1063/1.869691.

[22] Taylor JR, Sarkar S, Armenio V. Large eddy simulation of stably stratified open channel flow. Phys Fluids 2005;17:116602. http://dx.doi.org/10.1063/1.2130747.

[23] Tiselj I, Bergant R, Mavko B, Bajsic I, Hetsroni G. DNS of turbulent heat transfer in channel flow with heat conduction in the solid wall. Trans ASME J Heat Transfer 2001;123:849. http://dx.doi.org/10.1115/1.1389060.

[24] Zonta F, Marchioli C, Soldati A. Modulation of turbulence in forced convection by temperature-dependent viscosity. J Fluid Mech 2012;697:150. http://dx.doi.org/10.1017/jfm.2012.67.

[25] Zonta F, Onorato M, Soldati A. Turbulence and internal waves in stably-stratified channel flow with temperature-dependent fluid properties. J Fluid Mech 2012;697:175. http://dx.doi.org/10.1017/jfm.2012.51.

[26] Zonta F, Soldati A. Effect of temperature dependent fluid properties on heat transfer in turbulent mixed convection. Trans ASME J Heat Transfer 2013;136:022501. http://dx.doi.org/10.1115/1.4025135.